IOP Conference Series: Materials Science and Engineering

Study on Distribution of Magnetite (Fe3-xMn_xO_4) Filler in $Fe_{3-x}Mn_xO_4$-PEG/PVA/PVP Magnetic Hydrogel by Using Twolognormal Function Analysis

IOP Conf. Series: Materials Science and Engineering **515** (2019) 012024 doi:10.1088/1757-899X/515/1/012024

Study on Distribution of Magnetite ($Fe_{3-x}Mn_xO_4$) Filler in $Fe_{3-x}Mn_xO_4$-PEG/PVA/PVP Magnetic Hydrogel by Using Two-lognormal Function Analysis

Muchlis Fajar Hidayat[1], Sunaryono[1,2,*], Sujito[1], Nandang Mufti[1,2], Eny Latifah[1]

[1] Department of Physics, Faculty of Mathematics and Natural Sciences, Universitas Negeri Malang, Jl. Semarang 5, Malang 65145, Indonesia
[2] Center of Advanced Materials for Renewable Energy (CAMRY), Universitas Negeri Malang, Jl. Semarang 5, Malang 65145, Indonesia

*Corresponding author's email: sunaryono.fmipa@um.ac.id

Abstract. The trend of nanoparticles technology has been so advanced in several years; for instance, the bio-applications of polymer gel composites that involve micro/nanoparticles to be embedded in polymer gel have been many observed. This complex material composition can express a specific property and low toxicity so it can be used in various domain uses. Besides, the polymers material must possess certain properties to be utilized in the biomedical application (magnetic hyperthermia, cancer therapy, and food industry) such as flexible, biocompatibility, and water swallowability. Magnetite is nanoparticle with a unique property that can be utilized as a filler. The low toxicity of magnetite under the superparamagnetic condition is very useful in biomedical application. This research was succeeded to synthesize PVA/PVP polymer-based hydrogel magnetic with PEG-coated magnetite with Manganese doping filler, which has good biocompatibility and stable particle. An advanced characterization using XRD has shown the crystallite size about 9-11 nm with the magnetite phase confirmed from the sample. The SAXS analysis using two-lognormal functions exhibited primary and secondary particles around 2.40 and 9.74 nm that was well proven by TEM image analysis that showed a close value of the average particles size about 9.78 nm. From the SAXS and TEM analysis, it could be observed that the samples formed clusters from primary and secondary particles.

Keywords: $Fe_{3-x}Mn_xO_4$-PEG, PVA/PVP, magnetic hydrogel, SAXS analysis, two lognormal function

1. Introduction

Nanoparticles are increasingly becoming the focus of research highly developed by researchers due to their superior nature. Many kinds of nanoparticles being developed by researchers ranging from silica [1–5], cobalt [6–10], ZnO [11–13], and so forth. One of the nanoparticles that have low toxicity [14–16] and biocompatible [17–19] is magnetite so that it can be used in the biomedical field [20–23]. Practically, magnetite can be utilized as a filler material in the magnetic hydrogel to be subsequently used as actuator [24,25] or as artificial [26–28]. Besides, the magnetic hydrogel can be also used as the packaging for environmentally friendly food.

The need for food in the current era is increasing with the increase in the world population [29], where it is in line with the enhancement of the need for high-quality food. Besides, the urgency of the waste produced by the food wrapping is also massively discussed by many scientists [30]. Considering such problems, an environmentally friendly food packaging was developed by the ability to protect the food form environmental contamination that can give the information of the food condition in the real-time and the packaging waste produced is biodegradable [31–33]. One of the developments of this food packaging is the use of hydrogel polymer as the raw material. PVP and PVA polymers have been proven to have a biocompatible characteristic with the low toxicity level and it is biodegradable [34–40]. Meanwhile, the use of PVA and PVP simultaneously becomes the magnetic hydrogel is still rarely reported.

Magnetic hydrogel consists of two important parts namely filler and hydrogel polymer as the place in which the filler materials attach. The filler of hydrogel polymer can be originated from any nanoparticles that one of them is in the form of magnetite nanoparticles [41]. The previous research on the hydrogel magnetic that used magnetic nanoparticles was reported by Safronov *et al*. [42]. They explained that magnetic nanoparticles and PAAm polymer underwent a strong interaction when they were composed so that the agglomeration appeared. This case is different from the condition when the filler magnetic used came from magnetic nanoparticles that had less agglomeration. This research caused the hydrogel magnetic difficult to develop if it was subjected to an external magnetic field but having the higher shear modulus. Besides, Blyakhman *et al*. [43] reported that the addition of magnetite in the PAAm hydrogel could increase the mechanic strength of the hydrogel magnetic system even in proportion to the increase in the polymer bonds. This addition also influenced the Young modulus that was in line with the number of magnetites. The magnetization measurement also showed the magnetite percentage which was in line with the magnetization happening in the magnetic hydrogel. The magnetic fabrication has been also successfully conducted by Sunaryono *et al*. [44] that used the raw material of polyvinyl alcohol (PVA) and magnetite filler. The formed magnetite nanoparticles had the diameter between 13 – 32 nm because of the aggregation between the particles that also correlated to the magnetite filler concentration level in the polymer namely from 1% to 15% of the hydrogel weight. However, the study of the distribution of magnetite filler ($Fe_{3-x}Mn_xO_4$) in the magnetic hydrogel of $Fe_{3-x}Mn_xO_4$-PEG/PVA/PVP is rarely reported.

This research had the magnetite raw material as the filler due to its superior nature and superparamagnetic characteristic when its size under 10 nm [45–47]. The synthesis of magnetite particles in this research employed the method of simple degradation namely coprecipitation method. Besides, the use of surfactant could improve the monodispersity of the magnetite nanoparticles [48]. Thereby, this research fabricated the magnetite added with PEG polymer and dopped with Mn. This polymer has the ability to add the biocompatibility of the magnetite [49,50]. Meanwhile, Mn doping was carried out to increase the magnetic characteristic of the magnetite nanoparticles. Subsequently, the study of the distribution of magnetite nanoparticles ($Fe_{3-x}Mn_xO_4$) in the magnetic hydrogel of $Fe_{3-x}Mn_xO_4$-PEG/PVA/PVP was undertaken using SAXS instrument and analyzed using global fitting method through a two-lognormal model.

2. Methods

2.1. Synthesis of $Fe_{3-x}Mn_xO_4$-PEG-coated nanoparticles

Natural iron sand that was used as the source of magnetite was taken from Tulungagung District, Indonesia. Before synthesizing the magnetite nanoparticles, we first mixed the PEG and distilled water to make the surfactant. Magnetite powder as starting material was extracted from the iron sand using a permanent magnet. The certain amount of magnetite powder was then synthesized to nanoparticles through coprecipitation method because of its simplicity. The magnetite powder was initially dissolved in hydrochloric acid (HCl) then mixed with $MnCl_2$ and $PEG.H_2O$ using magnetic stirrer followed by the titration process using ammonium hydroxide (NH_4OH) to obtain the magnetite nanoparticles as precipitates. The precipitation yielded was then washed using distilled water until pH = 7 was reached.

The variables through the process were under controlled (temperature, reaction time, pH, and mixing speed).

2.2. Fabrication of $Fe_{3-x}Mn_xO_4$-PEG/PVA/PVP magnetic hydrogels

PVA/PVP hydrogels were prepared by dissolving a particular composition of the polymers powder to distilled water under the controlled temperature to increase the solubility of the hydrogels. The process was succeeded by the indicator of polymers form changing into a paste. The paste was then mixed again with the magnetite nanoparticles and stirred until became homogenous gels. This experiment used the composition of polymer PVA/PVP and distilled water about 40:100 with 15% of $Fe_{3-x}Mn_xO_4$-PEG filler. The yield of the mixture was then placed in a mold prepared before and continued to F-T process for 3h compared to 1.5h.

2.3. Characterization

To collect the phase and crystal structure data from the powder samples of $Fe_{3-x}Mn_xO_4$-PEG nanoparticles, a characterization using X-ray diffractometer (Philips X-Pert MPD diffractometer) was conducted under 0.02° scanning data step and in the range of CuKα (λ = 1.54) angular position (2θ) from 20° to 90°, and was done at room temperature. The morphology of $Fe_{3-x}Mn_xO_4$-PEG nanoparticles samples was characterized using a Transmission Electron Microscope (JEM1400 JEOL). In addition, a comparison between the size data results from XRD and SAXS analyses can be made for further investigation.

The characterization using synchrotron SAXS was performed at Siam Photon Laboratory of Synchrotron Light Research Institute (SLRI) of Thailand to obtain the $Fe_{3-x}Mn_xO_4$-PEG nanoparticles distribution as the filler inside the $Fe_{3-x}Mn_xO_4$-PEG/PVA/PVP Magnetic Hydrogels. The characterization was also conducted because of the non-destructive measurement and the ability to obtain the primary size of the magnetic hydrogel sample. The energy of X-ray on the range of 6 to 9 keV generated the intensity of the SAXS scattering X-ray showed as the scattering vector function, q, that can cover the momentum transfer from 0.12 nm^{-1} to 2 nm^{-1} then can be noted as $q = (4\pi/\lambda) \sin(\theta/2)$, where θ is the angle between the scattered and incident beams, and λ refers to the wavelength of the incident X-ray. The sample-to-detector distances (sdd) of CDD detector used in the SAXS measurement for the high and low q ranges were 1200 mm and 4500 mm respectively. The data collected from the SAXS characterization were then normalized using SAXSIT and also calibrated and made the correction between the sample and the background scattering intensities. The final result on using SAXSIT software was the merged data of two different scattering vector ranges. The next step in the SAXS analysis was performed using SASfit software (0.94.10 version); under the two-lognormal distribution function model, the primary and secondary particles size, as well as the fractal dimension and the particles aggregation before dispersing process into the hydrogel could be obtained.

3. Results and Discussion

The X-ray diffraction (XRD) patterns of all powder samples of $Fe_{3-x}Mn_xO_4$-PEG with various concentrations of dopant in the range of x = 0, 0.2, 0.4, and 0.6 are shown in Figure 1. The patterns produced indicated that the powder samples had a quite similar patterns data with pure magnetite from other reported file before which could be confirmed from the suitable peaks of standard magnetite (JCPDS file, PDF No.19-0629) [51]. The XRD patterns showed some peaks corresponding to the (2 2 0), (3 1 1), (4 0 0), (4 2 2), (5 1 1), (4 4 0), and (5 3 3) planes which became the indication of spinel cubic structure with space group *Fd3m* [44]. Besides that, a shifting happened to the diffraction peaks to the lower angle as the increasing of x presented by Figure 2, inferred that the increasing of lattice parameter because of the successful insertion of Mn^{2+} ion by replacing Fe^{2+} and Fe^{3+} ions were partially from $Fe_{3-x}Mn_xO_4$-PEG [52,53]. Another reason from the increase happening was the ionic radius of Mn^{2+} that was larger than Fe^{2+} and Fe^{3+} ionic radius [54]. The lattice parameters of powder sample $Fe_{3-x}Mn_xO_4$-PEG correspondingly increased from 8.3711 to 8.3939 Å due to the increase of x appropriate with another

report before [55]. The analysis of XRD using Rietica software [56] exhibited an average crystallite size about 9-11 nm.

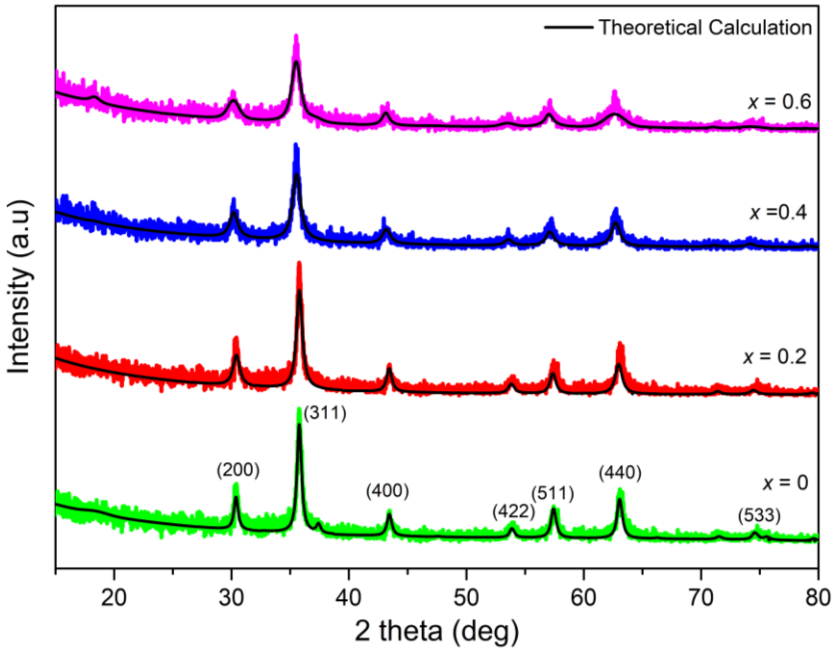

Figure 1. XRD patterns of $Fe_{3-x}Mn_xO_4$-PEG sample with various concentrations of dopant in the range of x = 0, 0.2, 0.4, and 0.6

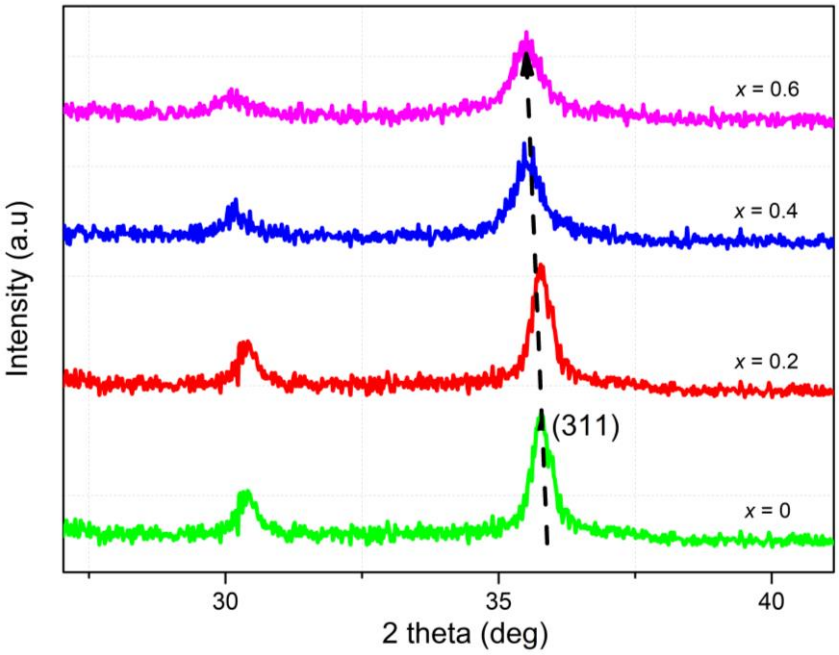

Figure 2. Profile of (311) peak shift of the powders sample of $Fe_{3-x}Mn_xO_4$-PEG sample with various concentrations of dopant in the range of x = 0, 0.2, 0.4, and 0.6

The complex system of magnetic hydrogel that consists of $Fe_{3-x}Mn_xO_4$-PEG nanoparticles as filler and polymer hydrogel PVA/PVP was characterized using SAXS and to investigate the aggregation of the nanoparticle $Fe_{3-x}Mn_xO_4$-PEG inside the magnetic hydrogel that included primary and secondary particles, the synchrotron data were analyzed using two-lognormal distribution function model to get the form factor of these particles. Besides that, two-lognormal distribution model also offers good information about the distribution of primary and secondary particles [44]. The function of the scattering vector (q) was used to calculate the scattering intensity in SAXS analysis with a certain relation between the scattering intensity $I(q)$, the form factor $P(q)$, and the structure factor $S(q)$ for particular N of $Fe_{3-x}Mn_xO_4$-PEG nanoparticles per unit volume that can be noted as follow.

$$I(q) = N_p P(q) S(q) + bkg \tag{1}$$

The morphology of the samples yielded from the characterization using TEM in this experiment showed that the nanoparticles formed fractal aggregates between one another that involved polydisperse nanoparticles (in cluster size) in which the cluster size distribution would have a limitation because of the process of aggregation. Moreover, the polydispersity will affect the difference of shape between the observed and the single cluster structure factor. The aggregate of the clustered object model which has a spherical particle formed a fractal-like cluster with ξ (correlation length) conforming to their whole size and D as the fractal dimension (self-similarity dimension) [57]. The structure factor of this system can be expressed by [58]

$$S(q,\xi,D,r) = 1 + \frac{D\Gamma(D-1)\sin\left(\left[D-1\right]\tan^{-1}(q\xi)\right)}{(qr_0)^D\left[1+(q\xi)^{-2}\right]^{(D-1)/2}} \tag{2}$$

The $Fe_{3-x}Mn_xO_4$-PEG/PVA/PVP magnetic hydrogel SAXS data were well-refined by SASfit software using two-lognormal distribution function shown in a good curve fitting in Figure 3 in the assumption that the system consisted of not only single size distribution. The two-lognormal equation is given in previous work [59]. The two-lognormal analysis result showed that the primary particles distribution of $Fe_{3-x}Mn_xO_4$-PEG dispersing inside the PVA/PVP hydrogel had the diameter of ~2.4 nm which had the similar result of the previous experimental report by Sun *et al*. [60] and Baumgartner *et al*. [61] that got the cluster aggregates with the diameter ~2.6 nm and 1-4 nm respectively.

In addition to the presence of primary particles, also there were secondary particles with the bigger size distribution about 9.74 nm; the diameter of these secondary particles was confirmed by the characterization using the image of transmission electron microscopy (TEM) which had been analyzed using ImageJ and Origin software; the analysis exhibited an average particle of 9.78 nm that had the similarity with the XRD crystallite size of $Fe_{3-x}Mn_xO_4$-PEG in this experiment (~9-11 nm) and from another experiment reported before [62,63]. The evidence of the aggregation process in magnetite nanoparticles is shown in Figure 4; it shows that the nanoparticles tended to cluster because of the strong pull force between one particle and another [64]. Another variable from equation (2) and (3) that contributed to the sample was D which referred to the fractal dimension of $Fe_{3-x}Mn_xO_4$-PEG, in the analysis the fractal dimension tends to 3 (~2.78 exactly), corresponding to the sample the structure that grew into three-dimensional building block [52]. The aggregation of $Fe_{3-x}Mn_xO_4$-PEG can be illustrated as Figure 5.

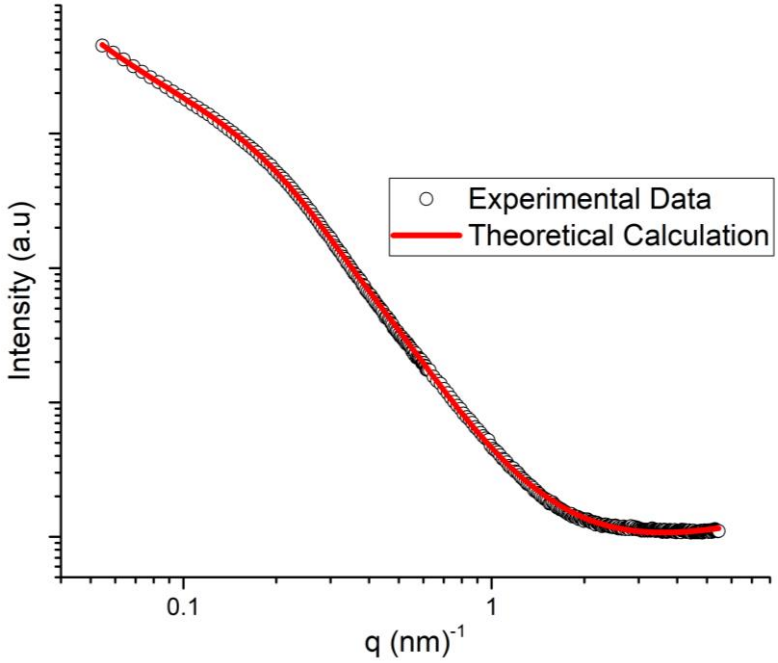

Figure 3. SAXS patterns of $Fe_{3-x}Mn_xO_4$-PEG nanoparticles inside magnetic hydrogel with the F-T process of 3 time

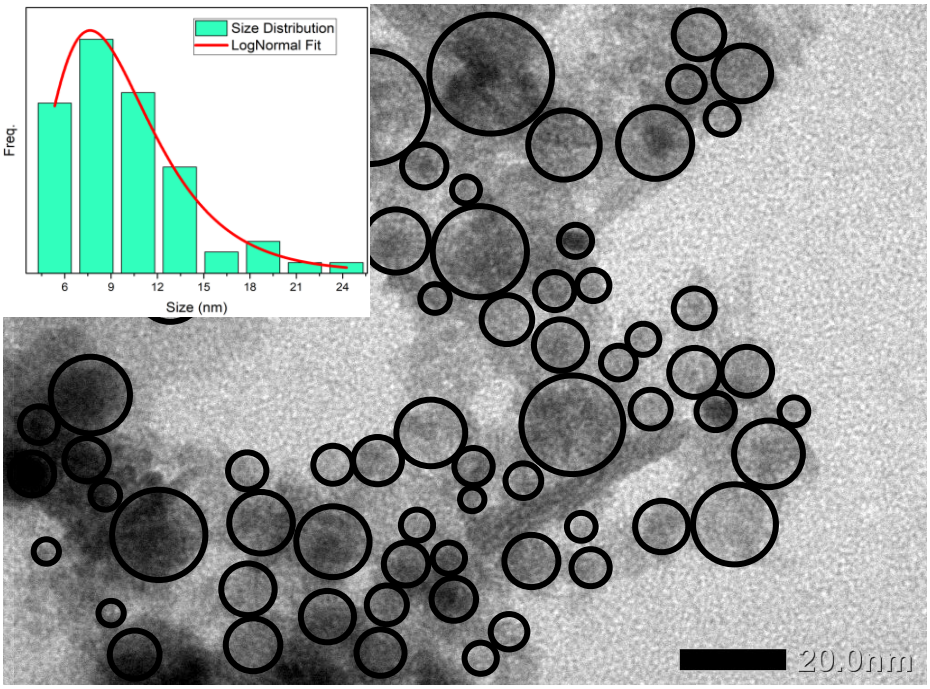

Figure 4. The TEM image of magnetite with particle size distribution

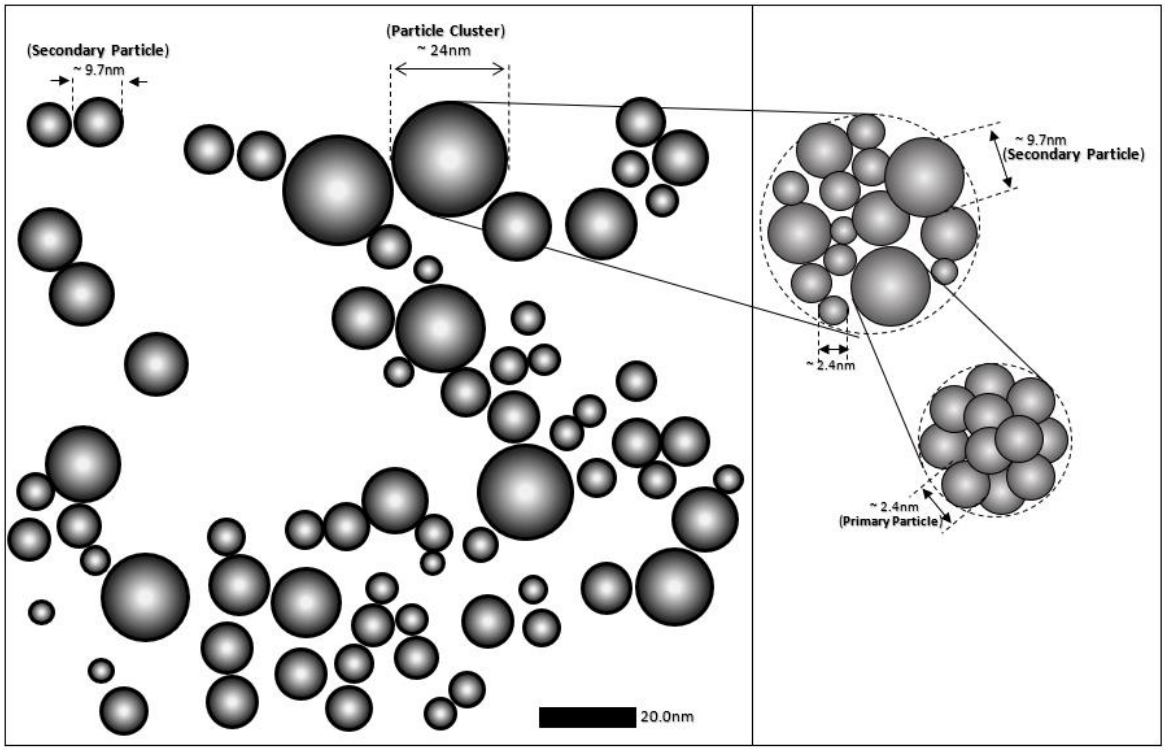

Figure 5. Schematic of $Fe_{3-x}Mn_xO_4$-PEG nanoparticles aggregation inside PVA/PVP hydrogel magnetic

4. Conclusion

The synthesis of $Fe_{3-x}Mn_xO_4$-PEG with x = 0, 0.2, 0.4, and 0.6 nanoparticles has been successfully conducted through coprecipitation method. The magnetite phase was well identified from $Fe_{3-x}Mn_xO_4$-PEG nanoparticles according to JCPDS file, PDF No.19-0629 with XRD patterns analysis result that showed the crystallite size about 9-11 nm. $Fe_{3-x}Mn_xO_4$-PEG/PVA/PVP magnetic hydrogel has been characterized by SAXS and analyzed using a two-lognormal function that produced the primary and secondary particle size ~2.4 nm and ~9.7 nm respectively; this result was well confirmed by the TEM image that exhibited the nanoparticles size about 9.8 nm polymeric.

References

[1] Bhattacharya M and Mandal M K 2018 Synthesis of rice straw extracted nano-silica-composite membrane for CO_2 separation *J. Clean. Prod.* **186** 241–52
[2] Borouni M, Niroumand B and Maleki A 2018 A study on crystallization of amorphous nano silica particles by mechanical activation at the presence of pure aluminum *J. Solid State Chem.* **263** 208–15
[3] Mohammed B S and Adamu M 2018 Mechanical performance of roller compacted concrete pavement containing crumb rubber and nano silica *Constr. Build. Mater.* **159** 234–51
[4] Yang B, Zhang Y, Xuan F Z, Xiao B, He L and Gao Y 2018 Improved adhesion between nickel–titanium SMA and polymer matrix via acid treatment and nano-silica particles coating *Adv. Compos. Mater.* **27** 331–48
[5] Zabihi N and Hulusi Ozkul M 2018 The fresh properties of nano silica incorporating polymer-modified cement pastes *Constr. Build. Mater.* **168** 570–9
[6] He R, Wang J, He M, Yang H and Ruan J 2018 Synthesis of WC composite powder with nano-cobalt coatings and its application in WC-4Co cemented carbide *Ceram. Int.* **44** 10961–7

[7] Amirthavalli C, Thomas J M, Nagaraj K and A.A.M. P 2018 Facile room temperature CTAB-assisted synthesis of mesoporous nano-cobalt ferrites for enhanced magnetic behaviour *Mater. Res. Bull.* **100** 289–94
[8] El-Khatib A M, Badawi M S, Roston G D, Khalil A M, Moussa R M and Mohamed M M 2018 Synthesis and Characterization of Cobalt Nanoparticles Prepared by Arc Discharge Method Using an Ultrasonic Nebulizer *J. Nano Res.* **52** 88–101
[9] Sridhar V and Park H 2018 Carbon encapsulated cobalt sulfide nano-particles anchored on reduced graphene oxide as high capacity anodes for sodium-ion batteries and glucose sensor *J. Alloys Compd.* **764** 490–7
[10] Sontu U B, G N R, Chou F C and M V R R 2018 Temperature dependent and applied field strength dependent magnetic study of cobalt nickel ferrite nano particles: Synthesized by an environmentally benign method *J. Magn. Magn. Mater.* **452** 398–406
[11] Guzman M, Flores B, Malet L and Godet S 2018 Synthesis and Characterization of Zinc Oxide Nanoparticles for Application in the Detection of Fingerprints **916** 232–6
[12] Kathiwada C P, Kaviyarasu K, Raman G and Swaminathan M 2018 The present work reports the green synthesis of Zinc Oxide Nanoparticles (ZnO NPs) *J. Photochem. Photobiol. B*
[13] Awan S U, Mehmood Z, Hussain S, Shah S A, Ahmad N, Rafique M, Aftab M and Abbas T A 2018 Correlation between structural, electrical, dielectric and magnetic properties of semiconducting Co doped and (Co, Li) co-doped ZnO nanoparticles for spintronics applications *Phys. E Low-Dimens. Syst. Nanostructures*
[14] Esmaeilpour M, Sardarian A R and Firouzabadi H 2018 Theophylline Supported on Modified Silica-Coated Magnetite Nanoparticles as a Novel , Efficient , Reusable Catalyst in Green One-Pot Synthesis of Spirooxindoles and Phenazines 9236–48
[15] Mayne R, Whiting J and Adamatzky A 2017 Toxicity and Applications of Internalised Magnetite Nanoparticles Within Live Paramecium caudatum Cells
[16] Zheng M, Lu J and Zhao D 2018 Science of the Total Environment Effects of starch-coating of magnetite nanoparticles on cellular uptake , toxicity and gene expression pro fi les in adult zebra fi sh *Sci. Total Environ.* **622**–**623** 930–41
[17] Kansara K, Patel P, Shukla R K, Pandya A, Shanker R, Kumar A and Dhawan A 2018 Synthesis of biocompatible iron oxide nanoparticles as a drug delivery vehicle *Int. J. Nanomedicine* **13** 79–82
[18] Yew Y P, Shameli K, Miyake M, Ahmad Khairudin N B B, Mohamad S E B, Naiki T and Lee K X 2018 Green biosynthesis of superparamagnetic magnetite Fe_3O_4 nanoparticles and biomedical applications in targeted anticancer drug delivery system: A review *Arab. J. Chem.*
[19] Klein S, Kızaloğlu M, Portilla L, Park H, Rejek T, Hümmer J, Meyer K, Hock R, Distel L V R, Halik M and Kryschi C 2018 Enhanced In Vitro Biocompatibility and Water Dispersibility of Magnetite and Cobalt Ferrite Nanoparticles Employed as ROS Formation Enhancer in Radiation Cancer Therapy *Small* **14** 1–10
[20] Kratz H, Taupitz M, De Schellenberger A A, Kosch O, Eberbeck D, Wagner S, Trahms L, Hamm B and Schnorr J 2018 Novel magnetic multicore nanoparticles designed for MPI and other biomedical applications: From synthesis to first in vivo studies *PLoS ONE* **13** 1–22
[21] Montazeran A H, Saber-samandari S and Khandan A 2018 Artificial intelligence investigation of three silicates bioceramics- magnetite bio-nanocomposite : Hyperthermia and biomedical applications **5** 163–71
[22] Chapa C, Lara D and García P 2019 *World Congress on Medical Physics and Biomedical Engineering 2018* vol 68/2 (Springer Singapore)
[23] Illés E, Szekeres M, Tóth I Y, Szabó Á, Iván B, Turcu R, Vékás L, Zupkó I, Jaics G and Tombácz E 2018 Multifunctional PEG-carboxylate copolymer coated superparamagnetic iron oxide nanoparticles for biomedical application *J. Magn. Magn. Mater.* **451** 710–20

[24] Yang Y, Tan Y, Wang X, An W, Xu S, Liao W and Wang Y 2018 Photothermal Nanocomposite Hydrogel Actuator with Electric-Field-Induced Gradient and Oriented Structure *ACS Appl. Mater. Interfaces* **10** 7688–92
[25] Chouhan D, Mehrotra S, Majumder O and Mandal B B 2018 Magnetic Actuator Device Assisted Modulation of Cellular Behavior and Tuning of Drug Release on Silk Platform *ACS Biomater. Sci. Eng.* acsbiomaterials.8b00240
[26] Adedoyin A A and Ekenseair A K 2018 Biomedical applications of magneto-responsive scaffolds
[27] Lawrence M B, Abbas S, Aswal V K and Lawrence M B 2018 Structure of polyvinyl alcohol-borax ferrogels : a small angle neutron scattering study *J. Polym. Res.* **25** (7 pp)
[28] Borin D, Chirikov D and Zubarev A 2018 Shear Elasticity of Magnetic Gels with Internal Structures *Sensors* **18** 2054
[29] Bereau P R 2018 World Population Datasheet: With a Special Focus on Changing Age Structures 20
[30] Han J-W, Ruiz-Garcia L, Qian J-P and Yang X-T 2018 Food Packaging: A Comprehensive Review and Future Trends *Compr. Rev. Food Sci. Food Saf.* **17** 860–77
[31] Pereda M, Marcovich N E and Ansorena M R 2018 Nanotechnology in Food Packaging Applications: Barrier Materials, Antimicrobial Agents, Sensors, and Safety Assessment *Handb. Ecomater.* 1–22
[32] Valentini L, Bittolo Bon S and Pugno N 2018 Combining Living Microorganisms with Regenerated Silk Provides Nanofibril-Based Thin Films with Heat-Responsive Wrinkled States for Smart Food Packaging *Nanomaterials* **8** 518
[33] Thakur V K and Thakur M K 2018 Polymer Gels: Science and Fundamentals (Springer)
[34] Zanela J, Bilck A P, Casagrande M, Victória M, Grossmann E and Yamashita F 2018 Polyvinyl alcohol (PVA) molecular weight and extrusion temperature in starch / PVA biodegradable sheets **5169** 256–65
[35] Basha S K S, Reddy K V B and Rao M C 2018 Optical absorption studies on biodegradable PVA/PVP blend polymer electrolyte system **050003** 050003
[36] Azad M U and Haque I 2018 Impact of Ytterbium Ion on Substantial Effects of **18**
[37] Kanca Y, Milner P, Dini D and Amis A A 2018 Tribological properties of PVA/PVP blend hydrogels against articular cartilage *J. Mech. Behav. Biomed. Mater.* **78** 36–45
[38] Cao L, Wu X, Wang Q and Wang J 2018 Biocompatible nanocomposite of TiO2incorporated bi-polymer for articular cartilage tissue regeneration: A facile material *J. Photochem. Photobiol. B* **178** 440–6
[39] Zidan H M, Abdelrazek E M, Abdelghany A M and Tarabiah A E 2018 Characterization and some physical studies of PVA/PVP filled with MWCNTs *J. Mater. Res. Technol.* 1–10
[40] Husain M S B, Gupta A, Alashwal B Y and Sharma S 2018 Synthesis of PVA/PVP based hydrogel for biomedical applications: a review *Energy Sources Part Recovery Util. Environ. Eff.* **40** 2388–93
[41] Safronov A P, Mikhnevich E A, Lotfollahi Z, Blyakhman F A, Sklyar T F, Larrañaga Varga A, Medvedev A I, Fernández Armas S and Kurlyandskaya G V. 2018 Polyacrylamide ferrogels with magnetite or strontium hexaferrite: Next step in the development of soft biomimetic matter for biosensor applications *Sens. Switz.* **18**
[42] Safronov A P, Shankar A, Mikhnevich E A and Beketov I V. 2018 Influence of the particle size on the properties of polyacrylamide ferrogels with embedded micron-sized and nano-sized metallic iron particles *J. Magn. Magn. Mater.* **459** 125–30
[43] Blyakhman F A, Buznikov N A, Sklyar T F, Safronov A P, Golubeva E V., Svalov A V., Sokolov S Y, Melnikov G Y, Orue I and Kurlyandskaya G V. 2018 Mechanical, electrical and magnetic properties of ferrogels with embedded iron oxide nanoparticles obtained by laser target evaporation: Focus on multifunctional biosensor applications *Sens. Switz.* **18**

[44] Sunaryono, Taufiq A, Mufti N, Susanto H, Putra E G R, Soontaranon S and Darminto 2018 Contributions of TMAH Surfactant on Hierarchical Structures of PVA/Fe_3O_4–TMAH Ferrogels by Using SAXS Instrument *J. Inorg. Organomet. Polym. Mater.*

[45] Kandasamy G, Sudame A, Bhati P, Chakrabarty A, Kale S N and Maity D 2018 Systematic magnetic fluid hyperthermia studies of carboxyl functionalized hydrophilic superparamagnetic iron oxide nanoparticles based ferrofluids *J. Colloid Interface Sci.* **514** 534–43

[46] Champagne P, Westwick H, Bouthillier A and Sawan M 2018 Colloidal stability of superparamagnetic iron oxide nanoparticles in the central nervous system : a review **13** 1385–400

[47] Yan L, Amirshaghaghi A, Huang D, Miller J, Stein J M, Busch T M, Cheng Z and Tsourkas A 2018 Protoporphyrin IX (PpIX)-Coated Superparamagnetic Iron Oxide Nanoparticle (SPION) Nanoclusters for Magnetic Resonance Imaging and Photodynamic Therapy *Adv. Funct. Mater.* **28** 1–8

[48] Li F and Han X 2018 One-pot synthesis of monodisperse magnetite in aqueous mixed surfactant solutions **020053** 020053

[49] Rosman R, Saifullah B, Maniam S, Dorniani D, Hussein M and Fakurazi S 2018 Improved Anticancer Effect of Magnetite Nanocomposite Formulation of GALLIC Acid (Fe_3O_4-PEG-GA) Against Lung, Breast and Colon Cancer Cells *Nanomaterials* **8** 83

[50] Hu J, Obayemi J D, Malatesta K, Košmrlj A and Soboyejo W O 2018 Enhanced cellular uptake of LHRH-conjugated PEG-coated magnetite nanoparticles for specific targeting of triple negative breast cancer cells *Mater. Sci. Eng. C* **88** 32–45

[51] Information S 2010 Assembly of Magnetite Nanoparticles into Spherical Mesoporous Aggregates with a 3-D Wormhole-Like Porous Structure 1–9

[52] Taufiq A, Sunaryono, Rachman Putra E G, Okazawa A, Watanabe I, Kojima N, Pratapa S and Darminto 2015 Nanoscale Clustering and Magnetic Properties of Mn x $Fe_{3-x}O_4$ Particles Prepared from Natural Magnetite *J. Supercond. Nov. Magn.* **28** 2855–63

[53] T. J. Malek1, S. H. Chaki, M. D. Chaudhary J P T and M P D 2018 Effect of Mn Doping on Fe_3O_4 Nanoparticles Synthesized by Wet chemical Reduction Technique *Iran. J. Energy Environ.* **9** 121–9

[54] Yang X, Kan J, Zhang F, Zhu M and Li S 2017 Facile Fabrication of Mn2+ Doped Magnetite Microspheres as Efficient Electrode Material for Supercapacitors *J. Inorg. Organomet. Polym. Mater.* **27** 542–51

[55] Amighian J, Karimzadeh E and Mozaffari M 2013 The effect of Mn2+substitution on magnetic properties of MnxFe3-xO4nanoparticles prepared by coprecipitation method *J. Magn. Magn. Mater.* **332** 157–62

[56] Howard C J, Hunter B A and Rietica B A 1997 A computer program for Rietveld analysis of X-ray and neutron powder diffraction patterns (Australian Nuclear Science and Technology Organisation, Menai) *Lucas Heights Res. Lab.*

[57] Putra E G R, Seong B S, Shin E, Ikram A, Ani S A and Darminto 2010 Fractal Structures on Fe $_3$ O $_4$ Ferrofluid: A Small-Angle Neutron Scattering Study *J. Phys. Conf. Ser.* **247** 012028

[58] Teixeira J 1987 Small angle scattering by fractal systems *Proceeding Int. Conf. Appl. Tech. Small Angle Neutron Scatt. Argonne Natl. Lab Oct. 26-29* 26–9

[59] Yusuf S M, Mukadam M D, De Teresa J M, Ibarra M R, Kohlbrecher J, Heinemann A and Wiedenmann A 2010 Structural and magnetic properties of amorphous iron oxide *Phys. B Condens. Matter* **405** 1202–6

[60] Sun S, Gebauer D and Cï¿½lfen H 2017 Alignment of Amorphous Iron Oxide Clusters: A Non-Classical Mechanism for Magnetite Formation *Angew. Chem. - Int. Ed.* **56** 4042–6

[61] Baumgartner J and Faivre D 2015 Iron solubility, colloids and their impact on iron (oxyhydr)oxide formation from solution *Earth-Sci. Rev.* **150** 520–30

[62] Vunain E, Mishra A K and Krause R W 2013 Fabrication, Characterization and Application of Polymer Nanocomposites for Arsenic(III) Removal from Water *J. Inorg. Organomet. Polym. Mater.* **23** 293–305
[63] Szabó T, Nánai L, Nesztor D, Barna B, Malina O and Tombácz E 2018 A Simple and Scalable Method for the Preparation of Magnetite/Graphene Oxide Nanocomposites under Mild Conditions *Adv. Mater. Sci. Eng.* **2018**
[64] Sunaryono, Taufiq A, Putra E G R, Okazawa A, Watanabe I, Kojima N, Rugmai S, Soontaranon S, Zainuri M, Triwikantoro, Pratapa S and Darminto 2016 Small-Angle X-Ray Scattering Study on PVA/Fe_3O_4 Magnetic Hydrogels *Nano* **11** 1650027

Acknowledgments
This research could be well conducted due to the financial support from *Hibah Penelitian Strategis Nasional* 2018 in the name of SN. The authors would like to thank DRPM KEMENRISTEKDIKTI RI that has supported this research.